Journal of Photochemistry and Photobiology A: Chemistry 203 (2009) 125–130

Contents lists available at ScienceDirect

Journal of Photochemistry and Photobiology A: Chemistry

journal homepage: www.elsevier.com/locate/jphotochem

Role of a phthalocyanine–fullerene dyad in multilayered organic solar cells

Paola Vivo*, Mikko Ojala, Vladimir Chukharev, Alexander Efimov, Helge Lemmetyinen

Department of Chemistry and Bioengineering, Tampere University of Technology, P.O. Box 541, FIN-33101 Tampere, Finland

ARTICLE INFO

Article history:
Received 27 November 2008
Received in revised form
23 December 2008
Accepted 31 December 2008
Available online 14 January 2009

Keywords:
Phthalocyanine–fullerene dyad
Organic solar cell
Photoinduced electron transfer

ABSTRACT

A double-bridged phthalocyanine–fullerene dyad (H_2Pc–C_{60}ee) was used as photo-active intramolecular donor–acceptor system in a layered organic solar cell. In this device, a poly(3-hexylthiophene) (PHT) film was used as electron donor, whereas either C_{60} or perylene tetracarboxylic diimide (PTCDI) film was selected as electron acceptor. The introduction of the dyad layer leads to an enhancement of the power conversion efficiency (η) in all the examples, mainly due to an increase of the open-circuit voltage. By introducing the dyad in PTCDI-containing cells, the efficiency (being 0.32%) was enhanced by almost three times compared to that of the reference (0.12%). In C_{60}-containing cells, the efficiency of the dyad sample (being 0.30%) was over one and half times higher than that of the reference in the absence of the dyad (0.18%). The role of such a dyad in the solar cells is discussed in detail.

1. Introduction

Molecular dyads, in which the photoactive donors are covalently linked to electron acceptor moieties, are interesting examples of photoinduced electron transfer (PET) systems [1–6]. Typically, these are characterized by long lifetimes of the charge separated (CS) state, which opens up a possibility to collect the charges at corresponding electrodes, thus generating photocurrent. Many examples of donor–acceptor (D–A) systems can be found in literature, as suitable candidates for organic photovoltaics [7–14].

In most of the reported PET studies, porphyrin–fullerene dyads are analyzed [1,5,15–25], and for many of such systems the efficient formation of a CS state is observed. Phthalocyanine chromophores have some advantages over the porphyrin ones since they absorb the light in a wider spectral region. Phthalocyanine and fullerene units show excellent and very well-known characteristics as donors and acceptors, respectively. Due to their exceptional electronic and optical properties, numerous examples of photovoltaic devices based on phthalocyanine and fullerene are presented in literature [26–31]. Phthalocyanine–fullerene (Pc–C_{60}) dyads appear particularly promising as D–A pairs for organic photovoltaics. Nevertheless, not many studies about Pc–C_{60} dyads are reported in literature, because the synthesis of such compounds is quite a challenging task. Particularly, the introduction of Pc–C_{60} dyads in organic solar cells is described only in a few works [10,12]. Neugebauer et al. [10] analyze the photophysics and photovoltaic device characteristics of a Pc–C_{60} dyad. Its introduction in a bulk-heterojunction solar cell leads to an improvement in the spectral match to the solar emission spectrum, though with a reduction in the short-circuit current under white illumination.

Recently, we have synthesized a new double-bridged phthalocyanine–fullerene dyad (H_2Pc–C_{60}ee), as described in [32]. Double-linked Pc–C_{60}pairs are more attractive than single-linker dyads since this characteristic is responsible for an intimate contact between the electron donor and the electron acceptor, and promotes an efficient charge separation. Photophysical properties of this dyad have been thoroughly studied both in solution [32,33] and in solid films [34]. These studies reveal that efficient intramolecular PET process takes place from phthalocyanine to fullerene, which leads to the formation of a CS state with nanosecond and microsecond lifetimes in solution and in solid films, respectively.

In this paper, the Pc–C_{60} dyad (H_2Pc–C_{60}ee) is introduced as spin-coated film in a bilayer cell between a donor and an acceptor layer. To the best of our knowledge, it is the first time that this kind of multilayered cell, where a dyad is sandwiched between an additional donor and acceptor layers, is proposed. The cell scheme resembles the idea of the multistep PET, occurring through several donors and acceptors, which can contribute to a CS state where charges are separated by a long distance, thus retarding the undesired back electron transfer [35–41].

In this work, the contribution of the H_2Pc–C_{60}ee dyad to the efficiency of solar cells, characterized by different donor and acceptor couples, is evaluated. The role of the dyad in the cells is discussed. It is worth mentioning that the obtained power conversion efficiency (η) values, though quite low, are comparable with those of similar unencapsulated layered cells in air, presented in literature. Hence, the main contribution of this work is to offer a strategy that can be further applied to more efficient devices.

* Corresponding author. Tel.: +358 3 31153636; fax: +358 3 31152108.
E-mail address: paola.vivo@tut.fi (P. Vivo).

1010-6030/$ – see front matter © 2009 Elsevier B.V. All rights reserved.
doi:10.1016/j.jphotochem.2008.12.030

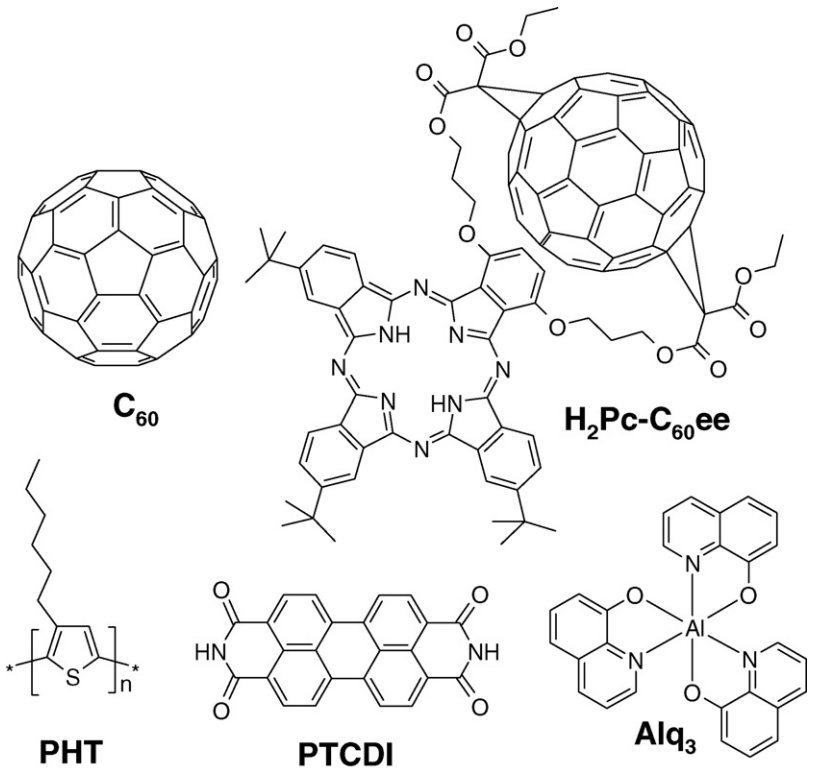

Fig. 1. Molecular structures of the organic compounds used as photo-active materials in the solar cells.

2. Experimental

The devices were fabricated on glass substrates coated with a transparent conducting Indium–Tin-Oxide (ITO) anode (Pgo-Germany). The ITO sheet resistance was about 8 Ω/ □. After a preliminary cleaning of the substrates, part of the ITO was removed from the plate by etching with aqua regia to prevent short circuit when contacting the cathode. Substrates were then cleaned with a detergent, rinsed 10 times with Milli-Q water, and finally cleaned in an ultrasonic bath (1 h in acetone and 1 h in isopropanol). Before use the plates were heated in N_2 flow at 150° C for 1 h and then a N_2 plasma cleaning process was applied for 10 min. The organic compounds (except the dyad) were commercially available (Sigma–Aldrich) and used without further purification. The phthalocyanine–fullerene dyad, $H_2Pc–C_{60}ee$ (1,4-bis[ethoxymalonateoxypropyloxy]-6(7),10(11),14(15)-tris[*tert* butyl]phthalocyanine-C_{60}), was synthesized as described in [32]. The molecular structures of all the compounds used are shown in Fig. 1.

Films preparation was performed by spin-coating at 2000 rpm for 60 s (PHT from a 2 g/l chloroform solution and $H_2Pc–C_{60}ee$ from a 4 g/l toluene solution), or by thermal evaporation under high vacuum (≈ 6×10^{-6} mbar) in an Edwards evaporation chamber (PTCDI, C_{60}, and Alq_3). PHT films were annealed after spin-coating in N_2 flow at 100° C for 30 min. The Au cathodes were evaporated through a mask to form cells with 1 mm^2 active area. The thicknesses of the active layers were estimated by calibration through a WYKO NT1100 profilometer. Thicknesses were 20 nm (PHT), 30 nm ($H_2Pc–C_{60}ee$), 35 nm (PTCDI and C_{60}), and 6 nm (Alq_3). Au thickness was approximately 70 nm. Except for the thermal evaporations, each other step of the device fabrication was performed in ambient conditions.

The structures of the measured devices are shown in Fig. 2. In devices **A** and **B**, PHT was used as donor layer and PTCDI as acceptor. In devices **C** and **D** the same donor (i.e., PHT) was used, while C_{60} was the acceptor. Samples **B** and **D** had an additional $H_2Pc–C_{60}ee$ layer between PHT and the acceptor. Finally, in all the devices, a thin layer of Alq_3 was adopted as buffer layer between the acceptor and the cathode, as proposed in [42].

One cell was manufactured (sample **E**), with similar structure as device **B**, but PHT and $H_2Pc–C_{60}ee$ were mixed in a chloroform solution, and then spin-coated on ITO as a single layer. In addition, devices **F**, **G**, **H**, **I** were prepared with Al cathode. A resume with the complete cell structure for all the prepared devices is presented in Table 1.

The current–voltage (*I–V*) characteristics in dark and under simulated AM 1.5 sunlight illumination (53 W/m^2) were measured by

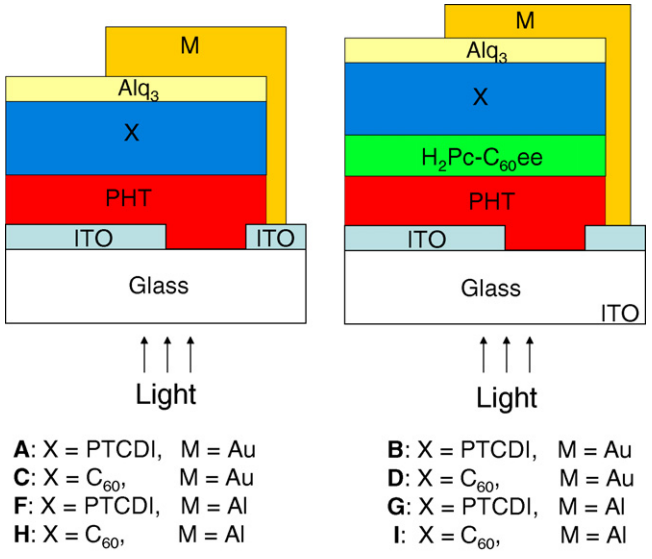

A: X = PTCDI, M = Au
C: X = C_{60}, M = Au
F: X = PTCDI, M = Al
H: X = C_{60}, M = Al

B: X = PTCDI, M = Au
D: X = C_{60}, M = Au
G: X = PTCDI, M = Al
I: X = C_{60}, M = Al

Fig. 2. Device layout of the investigated solar cells: without dyad (left), with dyad (right).

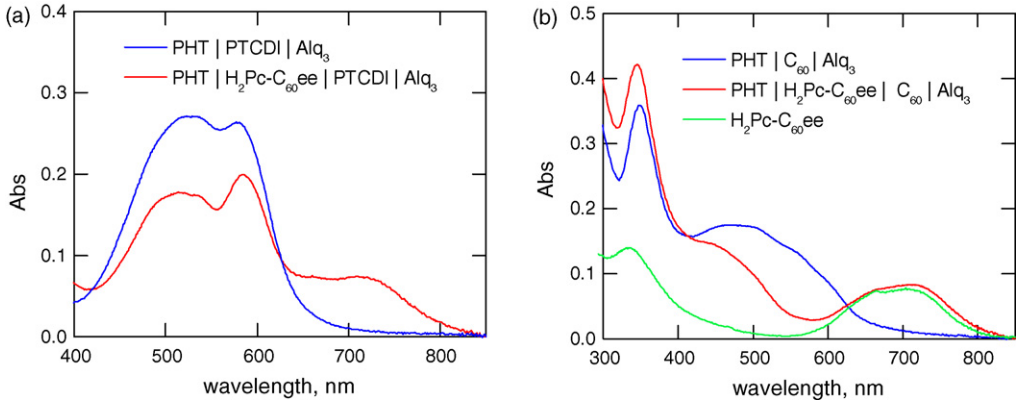

Fig. 3. (a) Absorption spectra of devices **A** and **B**; (b) absorption spectra of devices **C** and **D**. Absorption spectrum of the $H_2Pc–C_{60}ee$ dyad as spin-coated film from a 4 g/l toluene solution is also shown.

using E5272A source/monitor unit (Agilent). The AM 1.5 sunlight illumination was produced with a filtered Xe-lamp in the LZC-SSL solar simulator (Luzchem). All the measurements, including incident photon-to-current efficiency (*IPCE*) spectra, were carried out in air at room temperature, without encapsulation of the devices. The cells were illuminated with monochromatic light provided by a 75-W Xe-lamp model 71208 (Newport), and the wavelengths of the incident light were selected by a monochromator in the 400–800 nm range. The spectra were corrected using calibrated photodiodes.

3. Results and discussion

Absorption spectra of the main sample configurations (devices **A**, **B**, **C**, **D**) are presented in Fig. 3 a and b. In Fig. 3 b, the absorption spectrum of $H_2Pc–C_{60}ee$ spin-coated film is also shown. The device **B** absorption, as evaluated from the spectrum of Fig. 3, is slightly lower than that calculated by the superimposition of the absorption spectra of the individual components. Most deviation is observed around 500–600 nm, and it is due to the spin-coating of the dyad film on top of PHT, which is partly washed, and partly mixed with $H_2Pc–C_{60}ee$. However, such an absorption reduction seems not crucial to the photocurrent generation, even though a way to overcome this drawback will be proposed later in this Section.

Current–voltage (*I–V*) characteristics of the fabricated devices, in dark and under white illumination with 53 W/m^2, are shown in Fig. 4. All the samples present a good diode behaviour in the dark. When illuminated, the devices containing the dyad layer (devices **B** and **D**) exhibit better performances than the samples not containing the dyad (devices **A** and **C**). The main photovoltaic parameters derived from the *I–V* curves are summarized in Table 2. It is important to notice that the behaviour of different cells can be fairly compared, since the substrates have been etched and cleaned in the same run, and the common layers were spin-coated/evaporated at

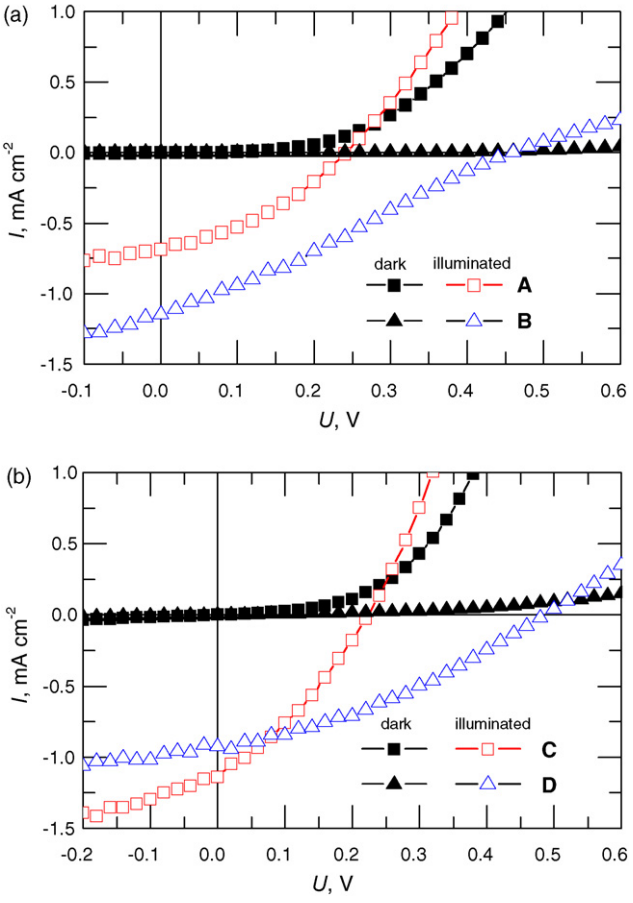

Fig. 4. Current (*I*) vs. voltage (*U*) characteristics in dark and under 53 W/m^2 simulated AM 1.5 solar illumination for devices **A**, **B**(a), and **C**, **D** (b).

Table 1
Structures of the devices analyzed in the present work.

Device	Cell structure
A	ITO | PHT | PTCDI |Alq_3|Au
B	ITO | PHT |$H_2Pc–C_{60}ee$ | PTCDI |Alq_3|Au
C	ITO | PHT |C_{60}|Alq_3|Au
D	ITO | PHT |$H_2Pc–C_{60}ee$ |C_{60}|Alq_3|Au
E	ITO |PHT:$H_2Pc–C_{60}ee$ | PTCDI |Alq_3|Au
F	ITO | PHT | PTCDI |Alq_3|Al
G	ITO | PHT |$H_2Pc–C_{60}ee$ | PTCDI |Alq_3|Al
H	ITO | PHT |C_{60}|Alq_3|Al
I	ITO | PHT |$H_2Pc–C_{60}ee$ |C_{60}|Alq_3|Al

Table 2
Short circuit current (I_{SC}), open-circuit voltage (U_{OC}), fill factor (*FF*), external power conversion efficiency (η), and incident-photon-to-current efficiency (*IPCE*) for devices **A**, **B**, **C**, **D**, and **E** obtained from *I–V* characteristics.

	I_{SC} (mA/cm^2)	U_{OC} (V)	*FF*	η (%)	*IPCE* (%)
Device **A**	0.69	0.25	0.35	0.12	3.18
Device **B**	1.15	0.45	0.28	0.32	5.33
Device **C**	1.14	0.21	0.35	0.18	4.82
Device **D**	0.93	0.50	0.34	0.30	3.94
Device **E**	2.50	0.33	0.24	0.40	11.1

the same time and from the same stock solutions (or dry materials).

Let us first refer to the couple of devices **A** and **B**, where PTCDI is adopted as acceptor layer. Device **B**, which contains the dyad layer, produces a current of 1.15 mA/cm^2 under illumination, while the reference device **A** produces only 0.69 mA/cm^2, i.e., almost half of the current. In spite of the lower absorbance in the central part of the spectrum ($\approx$ 500–600 nm), the generated photocurrent is higher in device **B**. This suggests that the reason for such a behaviour should be found in the significant contribution of the dyad absorption at 700 nm, which enlarges the absorption range of the dyad sample, compared to the reference. This cannot indeed be the only reason for the enhanced photocurrent, since the absorbance is quite low at 700 nm (around 0.1). The higher current is the main consequence of the facilitated electron movement from PHT to PTCDI through the dyad layer. In other words, the introduction of the dyad results in two different junctions in the cell (PHT |H_2Pc–C_{60}ee, and H_2Pc–C_{60}ee |PTCDI) instead of the one in PHT |PTCDI. The D–A pair acts as charge-sorting layer, thus contributing to a more efficient charge transport towards the electrodes.

A different behaviour was found to the other couple of samples (devices **C** and **D**). The reference **C** in this case shows a higher photocurrent (1.14 mA/cm^2) than that of the dyad sample (0.93 mA/cm^2). This can be explained by the fact that electrons are not so efficiently transferred from the fullerene moiety of the dyad to another fullerene layer (evaporated on top of it), but rather they are easily transported from PHT to C_{60}. Moreover, the fact that the current generated by the PHT |C_{60} cell is higher than that of PHT |PTCDI, results from the better matching of the PHT and C_{60} HOMO and LUMO energy levels (PHT: HOMO 5.2 eV, LUMO 3.0 eV; C_{60}: HOMO 6.2 eV; LUMO 3.6 eV) compared to those of PHT and PTCDI (PTCDI: HOMO 6.2 eV; LUMO 4.4 eV), as reported in literature [43–45].

The clear improvement in both dyad samples **B** and **D**, compared to the respective references, is the increase in the open-circuit voltage (U_{OC}), which is mostly responsible for the enhancement of the power conversion efficiency (η). By introducing the dyad in PTCDI-containing cells, η was enhanced by almost three times compared to that of the reference (from 0.12% up to 0.32%). In C_{60}-containing cells, η of the dyad sample (being 0.30%) was over one and half times higher than that of the reference in the absence of the dyad (0.18%). It must be emphasized that in the present work the device fabrication is not optimized, mainly as regards the thickness of the cell active layers. We have chosen thicknesses according to the values commonly reported in literature for these compounds, used in different device configurations. We believe that this is the main reason for the limited performances of the devices. The aim of the work is to prove the enhancement of η through the construction of a multilayered system containing a D–A pair, thus indicating that this Pc–C_{60} dyad is a promising material for photovoltaic application.

In order to understand the origin of the enhanced U_{OC} in the dyad samples, the role of the D–A pair in the cell should be described. A multistep PET process is expected to occur in a multilayered system. The primary electron transfer process takes place in the dyad layer, from the phthalocyanine moiety (yielding a cation) to the fullerene (yielding an anion). The PHT layer acts as antenna layer and secondary electron donor, which provides electrons to the dyad. PTCDI and C_{60} behave as secondary electron acceptors, taking electrons from the fullerene anion of the dyad, and at the same time as electron transporting layers (ETL). After electrons are transported to the last ETL layer, i.e., Alq_3, they are collected to the cathode. The main contribution to the charge separation is given by the D–A pair, thus being responsible for the generated additional voltage with respect to the reference sample. The CS process taking place in the dyad has been demonstrated by some steady-state and time-resolved spectroscopic measurements [34,46], in systems where the dyad and an antenna layer are studied. The time resolved Maxwell displacement charge (TRMDC) photovoltage measurements carried out on H_2Pc–C_{60}ee films show that the efficiency of the long-lived CS state formation in such a dyad is rather high. The CS state lifetime allows to collect the charges at the electrodes, and thus generate photocurrent [34].

The fill factor (*FF*) values (0.2–0.4) found in all the investigated cells are expected in these kind of devices where the active layer thicknesses are not optimized. In particular, the devices containing dyads have a slightly lower *FF* than the references, which can be explained by the higher series resistance due to the thicker active layer of this cell configuration.

Incident-photon-to-current efficiency (*IPCE*) spectra of the studied photovoltaic devices have been recorded, in order to find the components, which mostly affect the photocurrent generation. In Fig. 5 the normalized *IPCE* spectra, together with the corresponding absorption spectra, are presented. The same samples as for the white-light measurements have been used, and the spectra have been measured after $\approx$ 1 h of air exposure. The action spectra shapes resemble the absorption spectra quite well, thereby demonstrating that the present photocurrent generation is induced by the active layers. In Fig. 5 a, slightly higher efficiency is obtained for the reference sample **A** in the range 400–600 nm. However, a clear and significant contribution to the photocurrent is achieved in the 600–800 nm wavelength range in device **B**. The reason is the absorption of the dyad in this range. The D–A pair is capable to extend the absorption range of a sample, and thus to provide a better matching to the solar emission spectrum. In Fig. 5 b, a similar behaviour can be seen. For device **D**, the noticeable drop in the efficiency between 500 and 600 nm is compensated by the enhancement between 400–500 nm, and 600–800 nm.

Finally, *I–V* curves recorded with monochromatic light have been carried out on some samples (devices **A** and **B**), and the corresponding photovoltaic parameters (I_{SC}, U_{OC}, *FF*, external, Φ_E, and

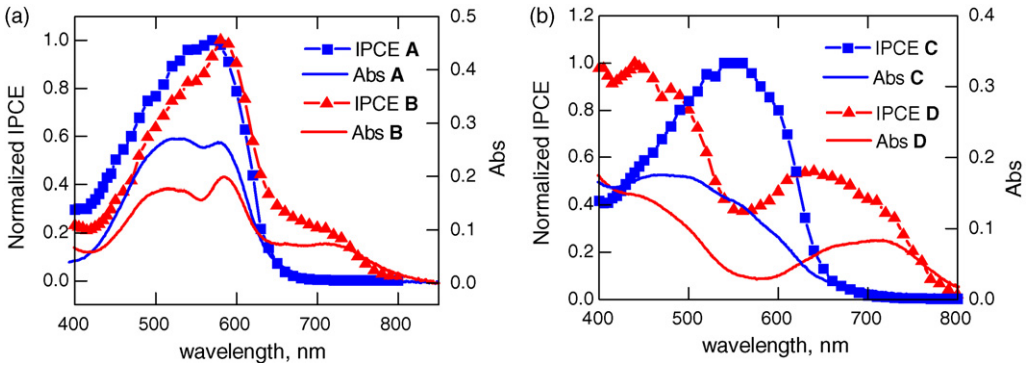

Fig. 5. Normalized incident-photon-to-current efficiency (*IPCE*) spectra and corresponding absorption (Abs) spectra for devices **A**, **B** (a), and **C**, **D** (b).

Table 3
Short circuit current (I_{SC}), open-circuit voltage (U_{OC}), fill factor (*FF*), external, Φ_E, and internal, Φ_I, quantum yields for devices **A** and **B**, obtained from *I–V* characteristics under monochromatic illumination.

	wl (nm)	I_{SC} (μA/cm^2)	U_{OC} (V)	*FF*	Φ_E (%)	Φ_I (%)
Device **A**	518	51.9	0.21	0.47	3.86	6.72
	540	57.5	0.21	0.48	4.19	7.85
	582	64.9	0.23	0.45	4.37	8.64
	700	0.25	0.05	0.26	0.02	0.56
Device **B**	518	46.3	0.31	0.29	3.44	5.93
	540	51.0	0.33	0.28	3.72	6.91
	582	63.4	0.35	0.28	4.27	8.23
	700	12.8	0.25	0.31	0.98	5.18

Measured on the same samples used for white-light measurements and *IPCE* spectra, after ≈ 2 h of air exposure.

internal, Φ_I, quantum yields) are reported in Table 3. Same samples as for white-light measurements and *IPCE* spectra were used, after ≈ 2 h of air exposure. The *I–V* curves were recorded at the excitation wavelengths of 518, 540, 582, and 700 nm, where the maxima in the absorption spectra lie (518 and 582 nm for PTCDI, 540 nm for PHT, and 700 nm for H_2Pc–C_{60}ee). These results support the conclusions obtained from the other experiments, which have been already described above. At the wavelengths where PHT and PTCDI mainly absorb, the reference generates slightly higher photocurrent, and thus higher quantum yields are achieved. The U_{OC} is always higher for device **B**, while *FF* is decreased, compared to device **A**. At 700 nm, the dyad sample exhibits over 50 times higher I_{SC} than the reference, and a corresponding huge increase in the quantum yield. H_2Pc–C_{60}ee is beneficial to the device efficiency, particularly due to the widening of the absorption of the device. The reduction in the absorption (and consequently in the generated photocurrent) in the central part of the spectrum due to technical reasons in the films preparation is the main reason for reduced efficiencies. In order to avoid the partial washing of the PHT layer caused by the dyad deposition (as explained in the first part of this Section), a mixed solution of PHT and H_2Pc–C_{60}ee is proposed for the spin-coating. The choice of the solvent is made according to the solubility of both compounds, and thus chloroform is selected. The resulting 1:1 mass mixture "PHT:H_2Pc–C_{60}ee" (with concentration 3 g/l) is then spin-coated, and the evaporated ETLs are deposited on top of it, before the Au evaporation. In Table 2 the results from the photocurrent measurements under white-light illumination are reported (device **E**). The highest efficiencies reported in this work are achieved with device **E**: η is 0.40%, and *IPCE* is 11.1% . It is worth mentioning that the absorption maximum at the dyad wavelengths (below 400 nm and above 650 nm) for device **E** is lower than that of device **B**, due to the lower concentration of the spin-coating solution. However, the generated photocurrent is higher. This result is explained by the wider absorption of the sample, which now significantly absorbs in the 500–600 nm wavelength range as well, underlying that the influence of PHT, and its interaction with H_2Pc–C_{60}ee, is relevant to the photocurrent generation.

For the sake of comparison, solar cells with Al cathode instead of Au cathode were also prepared and measured (see Table 4). The samples had same active layers as devices **A**–**D**, with the only difference being the top cathode. It is worth mentioning that these

Table 4
Photovoltaic parameters for devices **F**, **G**, **H**, and **I** with Alq_3/Al cathode, obtained from *I–V* characteristics.

	I_{SC} (mA/cm^2)	U_{OC} (V)	*FF*	η (%)	IPCE (%)
Device **F**	0.33	0.24	0.35	0.05	1.46
Device **G**	0.60	0.40	0.24	0.11	2.65
Device **H**	0.09	0.17	0.19	0.006	0.40
Device **I**	0.10	0.35	0.20	0.02	0.50

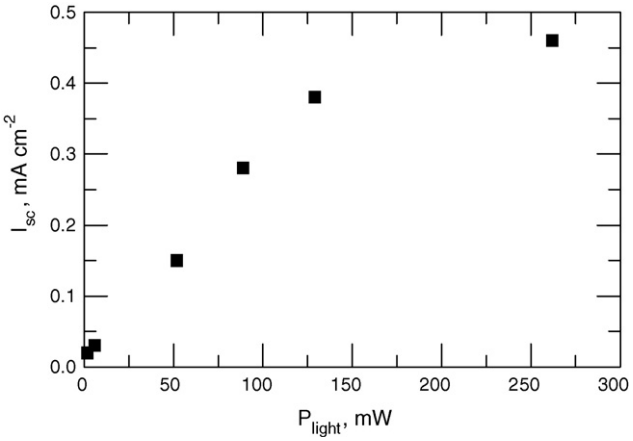

Fig. 6. Short circuit current (I_{SC}) vs. variable light intensity (P_{in}) for sample **B**. A similar trend was obtained for all the other samples.

Al-samples were protected from the outside atmosphere by being placed in a N_2-box right after preparation. Hence the influence of oxygen, which is a source of degradation for the Al, was suppressed since the samples were constantly under N_2 flow. Samples with Al cathode showed lower efficiencies than Au-cathode cells, even though keeping the same trend (Table 4). In fact, dyad samples always presented better performances than the corresponding references. The lower efficiencies obtained with Al cathode could at first sound surprising, since Al work function is better matching than Au with the ITO work function. This result indicates that the work function of the top cathode is not completely determined by the metal itself, but it is affected significantly by the presence of the Alq_3 layer, which mixes with the metal resulting in a different cathode work function [42]. In the case of Au, Alq_3 seems to lower its work function, thus facilitating the electron transport towards the cathode.

Finally, in order to investigate how the short-circuit current varies with the incident light power (P_{in}) as well as to clarify the mechanism of the sample excitation, some tests with variable incident light intensity were carried out. *I–V* dependencies were recorded at different intensities of the white light, by using gray filters with known transmittance. The I_{SC} values were plotted versus variable P_{in}, Fig. 6. Identical trends were observed for all the samples: for low values of P_{in}, a roughly linear trend can be found; at higher intensities (over 150 mW/cm^2) the photocurrent shows a saturation behaviour leading to a loss of cell efficiency. These results are in agreement with previously reported works [47,48] and suggest that the saturation is due to the exciton–exciton annihilation.

4. Conclusions

In summary, a multilayered Au-cathode organic solar cell in air was developed, with a spin-coated phthalocyanine–fullerene dyad (H_2Pc–C_{60}ee) layer between a donor (PHT) and acceptor (PTCDI or C_{60}). The dyad-containing devices exhibited higher efficiencies, compared to the references. By introducing the dyad in PTCDI-containing cells, η (being 0.32%) was enhanced by almost three times compared to that of the reference (0.12%). In C_{60}-containing cells, the η of the dyad sample (being 0.30%) was over one and half times higher than that of the reference in the absence of the dyad (0.18%). The main reason for such an enhancement was the increase in the open-circuit voltage. Moreover, the dyad widened the absorption spectrum of the sample, contributing to a better matching with the solar spectrum. The reported results indicate that phthalocyanine–fullerene dyads are a promising class of materials for organic photovoltaic applications.

All the devices described in the present work have been completely prepared and characterized in air, and the active layer thicknesses needs further optimization. Hence, the obtained efficiencies were quite low if compared to highest values of state-of-the-art devices. The highest efficiencies ($\eta = 0.40\%$, $IPCE = 11.1\%$) were obtained for a device where a 1:1 PHT:H_2Pc–C_{60}ee mixed layer was used.

We believe that more efficient devices can be prepared by optimizing the fabrication of the cells.

Acknowledgment

This work was supported by the Finnish Funding Agency for Technology and Innovation (TEKES), Project “Organic Solar Cells”.

References

[1] D. Kuciauskas, S. Lin, G.R. Seely, A.L. Moore, D. Gust, T. Drovetskaya, C.A. Reed, P.D.W. Boyd, J. Phys. Chem. 100 (1996) 15926–15932.
[2] D. Gust, T.A. Moore, A.L. Moore, Acc. Chem. Res. 34 (2001) 40–48.
[3] H. Imahori, D.M. Guldi, K. Tamaki, Y. Yoshida, C. Luo, Y. Sakata, S. Fukuzumi, J. Am. Chem. Soc. 123 (2001) 6617–6628.
[4] V. Vehmanen, N.V. Tkachenko, A.Y. Tauber, P.H. Hynninen, H. Lemmetyinen, Chem. Phys. Lett. 345 (2001) 213–218.
[5] H. Imahori, S. Fukuzumi, Adv. Funct. Mater. 14 (2004) 525–536.
[6] N. Mataga, H. Chrosrowjan, S. Taniguchi, J. Photochem. Photobiol. C 6 (2005) 37–79.
[7] N. Tagmatarchis, M. Prato, Struct. Bond. 109 (2004) 1–39.
[8] M.E. Milanesio, M. Gervaldo, L.A. Otero, L. Sereno, J.J. Silber, E.N. Durantini, J. Phys. Org. Chem. 15 (2002) 844–851.
[9] G. Possamai, M. Maggini, E. Menna, G. Scorrano, L. Franco, M. Ruzzi, C. Corvaja, G. Ridolfi, P. Samor, A. Geri, N. Camaioni, Appl. Phys. A 79 (2004) 51–58.
[10] H. Neugebauer, M.A. Loi, C. Winder, N.S. Sariciftci, G. Cerullo, A. Gouloumis, P. Vázquez, T. Torres, Solar Energy Mater. Solar Cells 83 (2004) 201–209.
[11] F. Meng, J. Hua, K. Chen, H. Tian, L. Zuppiroli, F. Nuesch, J. Mater. Chem. 15 (2005) 979–986.
[12] M.A. Loi, P. Denk, H. Hoppe, H. Neugebauer, C. Winder, D. Meissner, C. Brabec, N.S. Sariciftci, A. Gouloumis, P. Vázquez, T. Torres, J. Mater. Chem 13 (2003) 700–704.
[13] M. Maggini, G. Possamai, E. Menna, G. Scorrano, N. Camaioni, G. Ridolfi, G. Casalbore-Miceli, L. Franco, M. Ruzzi, C. Corvaja, Chem. Commun. 18 (2002) 2028–2029.
[14] H. Yamada, H. Imahori, Y. Nishimura, I. Yamazaki, T.K. Ahn, S.K. Kim, D. Kim, S. Fukuzumi, J. Am. Chem. Soc. 125 (2003) 9129–9139.
[15] H. Imahori, K. Hagiwara, M. Aoki, T. Akiyama, S. Taniguchi, T. Okada, M. Shirakawa, Y. Sakata, J. Am. Chem. Soc. 118 (1996) 11771–11782.
[16] D.I. Schuster, Carbon 38 (2000) 1607–1614.
[17] S. Fukuzumi, H. Imahori, H. Yamada, M.E. El-Khouly, M. Fujitsuka, O. Ito, D.M. Guldi, J. Am. Chem. Soc. 123 (2001) 2571–2575.
[18] F. D'Souza, S. Gadde, M.E. Zandler, K. Arkady, M.E. El-Khouly, M. Fujitsuka, O. Ito, J. Phys. Chem. A 106 (2002) 12393–12404.
[19] T.J. Kesti, N.V. Tkachenko, V. Vehmanen, H. Yamada, H. Imahori, S. Fukuzumi, H. Lemmetyinen, J. Am. Chem. Soc. 124 (2002) 8067–8077.
[20] N.V. Tkachenko, H. Lemmetyinen, J. Sonoda, K. Ohkubo, T. Sato, H. Imahori, S. Fukuzumi, J. Phys. Chem. A 106 (2003) 8834–8844.
[21] H. Imahori, K. Tamaki, D.M. Guldi, C. Luo, M. Fujitsuka, O. Ito, Y. Sakata, S. Fukuzumi, J. Am. Chem. Soc. 123 (2001) 2607–2617.
[22] F. D'Souza, R. Chitta, S. Gadde, A.L. McCarty, P.A. Karr, M.E. Zandler, A.S.D. Sandanayaka, Y. Araki, O. Ito, J. Phys. Chem. B 110 (2006) 5905–5913.
[23] P.D.W. Boyd, C.A. Reed, Acc. Chem. Res. 38 (2005) 235–242.
[24] T. Hasobe, P.V. Kamat, M.A. Absalom, Y. Kashiwagi, J. Sly, M.J. Crossley, K. Hosomizu, H. Imahori, S. Fukuzumi, J. Phys. Chem. B 108 (2004) 12865–12872.
[25] D.M. Guldi, Pure Appl. Chem. 75 (2003) 1069–1075.
[26] P. Peumans, S.R. Forrest, Appl. Phys. Lett. 79 (2001) 126–128.
[27] D. Gebeyehu, D.B. Maennig, J. Drechsel, K. Leo, M. Pfeiffer, Sol. Energy Mat. Solar Cells 79 (2003) 81–92.
[28] R. Koeppe, N.S. Sarifitci, P.A. Troshin, R.N. Lyubovskaya, Appl. Phys. Lett. 87 (2005) 244102.
[29] M.A. Loi, P. Denk, H. Hoppe, H. Neugebauer, D. Meissner, C. Winder, C.J. Brabec, N.S. Sariciftci, A. Gouloumis, P. Vázquez, T. Torres, Synth. Met. 137 (2003) 1491–1492.
[30] K. Suemori, T. Miyata, M. Yokoyama, M. Hiramoto, Appl. Phys. Lett. (2005) 063509.
[31] Z.R. Hong, B. Maennig, R. Lessmann, M. Pfeiffer, K. Leo, Appl. Phys. Lett. 90 (2007) 203505.
[32] M. Isosomppi, N.V. Tkachenko, A. Efimov, H. Vahasalo, J. Jukola, P. Vainiotalo, H. Lemmetyinen, Chem. Phys. Lett. 430 (2006) 36–40.
[33] M. Niemi, N.V. Tkachenko, A. Efimov, H. Lehtivuori, K. Ohkubo, S. Fukuzumi, H. Lemmetyinen, J. Phys. Chem. A 112 (2008) 6884–6892.
[34] H. Lehtivuori, T. Kumpulainen, A. Efimov, H. Lemmetyinen, A. Kira, H. Imahori, N.V. Tkachenko, J. Phys. Chem. C 112 (2008) 9896–9902.
[35] D. Gust, T.A. Moore, Science 244 (1989) 35–41.
[36] M.R. Wasielewski, Chem. Rev. 92 (1992) 435–461.
[37] C. Luo, D.M. Guldi, H. Imahori, K. Tamaki, Y. Sakata, J. Am. Chem. Soc. 122 (2000) 6535–6551.
[38] G. Kodis, P.A. Liddell, L. de la Garza, P.C. Clausen, J.S. Lindsey, A.L. Moore, T.A. Moore, D. Gust, J. Phys. Chem. A 106 (2002) 2036–2048.
[39] H. Imahori, Y. Mori, Y. Matano, J. Photochem. Photobiol. C 4 (2003) 51–83.
[40] P.A. Liddell, G. Kodis, L. de la Garza, A.L. Moore, T.A. Moore, D. Gust, J. Phys. Chem. B 108 (2004) 10256–10265.
[41] F. D'Souza, P.M. Smith, S. Gadde, A.L. McCarty, M.J. Kullman, M.E. Zendler, M. Itou, Y. Araki, O. Ito, J. Phys. Chem. B. 108 (2004) 11333–11343.
[42] P. Vivo, J. Jukola, M. Ojala, V. Chukharev, H. Lemmetyinen, Sol. Energy Mater. Solar Cells 92 (2008) 1416–1420.
[43] S. Oh, H.W. Rhee, C. Lee, Y.C. Kim, J.K. Kim, J.W. Yu, Curr. Appl. Phys. 5 (2005) 55–58.
[44] B. Rand, D. Burk, Phys. Rev. B 75 (2007) 115327.
[45] A.K. Pandey, J.M. Nunzi, Appl. Phys. Lett. 90 (2007) 263508.
[46] H. Lehtivuori, T. Kumpulainen, M. Hietala, A. Efimov, H. Lemmetyinen, A. Kira, H. Imahori, N.V. Tkachenko, J. Phys. Chem. C, 2009, in press, doi:10.1021/jp8061916.
[47] J. Gao, F. Hide, H. Wang, Synth. Met. 84 (1997) 979–980.
[48] D. Gebeyehu, C.J. Brabec, F. Padinger, T. Fromherz, J.C. Hummelen, D. Badt, H. Schindler, N.S. Sariciftci, Synth. Met. 118 (2001) 1–9.